Kinematic Analysis of Lumbar Spine Undergoing Extension and Dynamic Neural Foramina Cross Section Measurement

Yongjie Zhang[1], Boyle C. Cheng[2], Changho Oh[1], Jessica L. Spehar[2]
James Burgess[3]

Summary

The spinal column plays a vital biomechanical role in the human body by providing structural support and facilitating motion. As degenerative changes occur in the spine, however, chronic pain can result which frequently forces patient to seek surgical treatment. Such treatments seek to address that pain, frequently by addressing both spinal motion and structural integrity.

Spinal implant devices are designed to either restrict motion, e.g., fusion constructs, or preserve motion in a functional spinal unit such as spinal arthroplasty devices. Recent motion restriction designs have allowed new surgical intervention strategies such as interspinous process spacers. The efficacy of these devices has been established clinically and appears to rest on their ability to restrict or minimize motion while unfolding ligamentous structures that, if unchecked, leads to neural compression and disability. In this study, we used novel image processing techniques to characterize the performance of interspinous spacers in addition to standard biomechanical methods of comparison such as range of motion (ROM). Controlled bending protocols for flexibility testing were applied and the three dimensional kinematic response was measured.

A sequence of fluoroscopy imaging data were recorded during the flexibility protocol with an interspinous process spacer device placed at L2-L3. A fast marching method and the principal component analysis were developed and utilized for kinematics analysis of lumbar spine undergoing flexion extension bending and dynamic measurement of neural foramina cross section that ideally would be applicable to patient datasets. The implanted level exhibited a major reduction in ROM (approximately 10.4% compared to the intact state in flexion extension bending) but minor change in cross sectional foramina area (about 5.6%). Effectiveness of such devices in extension bending is important from a translational medicine point of view and requires information beyond ROM measures alone.

Introduction

The spinal column is one of the most vital structural components of the human body, supporting our trunks and making all of our movements possible. Degenerative ailments of the spine occur over time as the spinal components become

---

[1]Department of Mechanical Engineering, Carnegie Mellon University, Pittsburgh, PA 15213

[2]Department of Neurological Surgery, University of Pittsburgh, Pittsburgh, PA 15213

[3]Department of Neurosurgery, Allegheny General Hospital, Pittsburgh, PA 15212

worn from everyday use. The most frequent components involved include the intervertebral disc and the facet joints. These are our particular area of interest. As one of the routes of clinical treatment, medical device implant such as interspinous process spacer may be an effective way to relieve back pain due to processes that involve degeneration of both the intervertebral discs and the facets. This approach is particularly valuable for patients that would not tolerate more invasive surgical procedures.

Spinal implant devices are designed to either restrict motion or preserve motion in a functional spinal unit. Interspinous spacers reduce motion and hold the spinal motion segment in an optimized position. The recent interest in interspinous process spacers has been due in part to the relief of pain symptoms for patients when a stenotic lumbar segment is in a forward flexed position. These implants that restrict motion in extension are known to relieve the effects of intermittent neurogenic claudication. Methods of characterizing their performance must augment current characterization that were derived from fixation standards, i.e., range of motion (ROM). Developing and utilizing novel image processing techniques may potentially lead to better solutions for evaluating the efficacy of these devices on the ability to restrict or minimize abnormal motion. In this paper, we will utilize the fast marching method and principal component analysis to accurately characterize the performance of interspinous spacers in addition to standard biomechanical methods of comparison. Controlled bending protocols for flexibility testing were applied and the three dimensional kinematic response was measured.

Anatomy Structure of Lumbar Spine

As shown in Figure 1 [1], lumbar spine refers to the lower region of the spine directly below the cervical and thoracic regions and directly above the sacrum and mainly consists of a vertebral body, pedicles, laminae, facet joints, spinous process, and transverse processes. The lumbar spine has five lumbar vertebrae, $L1$-$L5$, and each lumbar vertebra is comprised of a vertebral body and a vertebral arch. The vertebral body is the thick oval segment of bone forming the front of the vertebral segment.

The vertebral body is shaped like an hourglass, thinner in the center with thicker ends and has a hard and strong outer-shell composed of cortical bone. The vertebral arch consists of 1) a pair of pedicles which are short stout transverse processes that project from the sides of the vertebral body and 2) a pair of laminae, the flat plates extending from the pedicles which together form the arch. The vertebral arch encloses the spinal canal. Facets are the joints that interconnect the vertebral arches and help with twisting motions and rotation of the spine. The surfaces of the facet joints are covered with cartilage that help the joints glide with minimal friction against one another. The spinous process projects from the joint of the two

laminae and these are the ridges which can be felt along the backbone. Transverse processes extend from the junction of the pedicles and lamina.
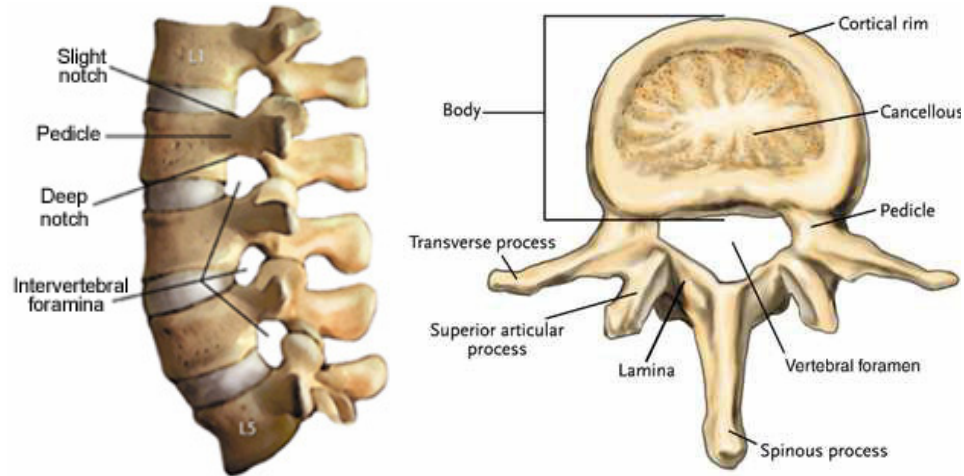

Figure 1: Anatomy of lumbar spine (http://www.back.com/anatomy-lumbar.html).

Computational Methods

A fresh frozen human cadaveric specimen was prepared for biomechanical flexibility testing. The segment includes *L*1-*S*1 and all soft tissue except for the osteoligamentous structures was removed. The spine was subjected to flexion extension bending at 7.5Nm on an automated spine tester. *L*2-*L*3 was instrumented with an interspinous spacer that was designed to restrict motion primarily in one direction. The 3D kinematic motion was recorded for 3 cycles with the third cycle analyzed for ROM. Additionally, high resolution dynamic fluoroscopic imaging captures the motion moving from flexion to extension of the third cycle. This information was then analyzed for vertebral body motion and foramina cross section area based on the mean of images in the forward flexion frames and the mean of images in the extension frames through a fast marching algorithm and principal component analysis.

The initial phase of the study began with segmenting the vertebral body (e.g., *L*2) and the foramina area (e.g., the foramina region between *L*1 and *L*2) in the 736 fluoroscopic images. The fast marching method [2-4] was chosen. Some seed points were selected in the regions of interest, and a contour was initialized and allowed to grow until a certain stopping condition was reached. Every voxel was assigned with a value called time and denoted by T, which was initially zero for all the seed points and infinite for all other voxels. Repeatedly, the voxel on the marching contour with minimal time value was deleted from the contour and the time values of its neighbors were updated. The gradient of arrival time was inversely

proportional to the growing speed of the isocontour, therefore the time function T satisfies the following equation:

$$\|\nabla T(x,y)\| \bullet F(x,y) = 1 \qquad (1)$$

where $F(x,y) = e^{-\alpha\|\nabla I\|}$ is the speed function determined by the gradients of the input maps I ($\alpha > 0$). The resulting segmentation of the vertebral body $L2$ at time step 1 and 736 are shown in Figure 2.
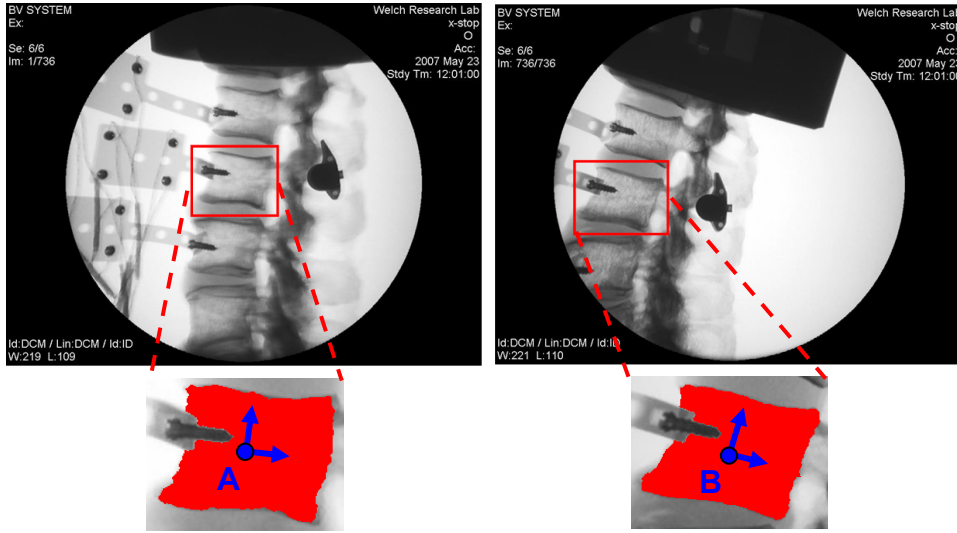

Figure 2: Segmented results of lumbar spine vertebral body L2 undergoing extension. Left – before extension; Right – after extension. Point A and B are two centroid points, and blue arrows represent two principle directions of the segmented regions (red ones).

If the ith red pixel in this segmented image has coordinates a_i (represented as row vector), we can estimate the center and orientation of the segmented image using the principal component analysis. The centroid c of the segmented region has coordinates $\frac{1}{n}\sum_{i=1}^{n} a_i$ where n is the number of red pixels. To estimate the orientation of the segmented region, we next form the 2×2 covariance matrix M:

$$M = \frac{1}{n}\sum_{i=1}^{n}(a_i - c)^T (a_i - c). \qquad (2)$$

The two eigenvectors of M are orthogonal, and they describe the directions of

the first and second principal variation of the data points. Together with the centroid *c*, these axes represent a coordinate system for the segmented image. Figure 2 shows the calculated results of the centroids and two principle directions before/after extension. By comparing those results, we can obtain an affine transformation to translate and rotate one onto the other. In Figure 3, the centroid point and two principal directions are calculated for the segmented *L2* and *L3*: (A^2,

Figure 3: The instantaneous rotation center.

n_1^2, n_2^2) for L2 and (A^3, n_1^3, n_2^3) for L3. The instantaneous rotation center O can be obtained from the following equation:
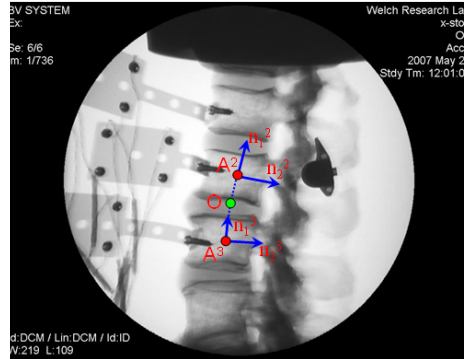
$$\begin{cases} \overrightarrow{OA^2} \cdot n_2^2 = 0 \\ \overrightarrow{OA^3} \cdot n_2^3 = 0 \end{cases} \qquad (3)$$

Figure 4 shows the resulting segmentation of the foramina cross sections at time step 1 and 732. The second phase of the study examined the area change during the flexion extension bending. Suppose *n* is the number of red pixels inside the segmented foramina region, then the foramina area is defined as $n \times \Delta x \times \Delta y$, where Δx and Δy are spacing of the imaging data along the *x* and *y* directions.
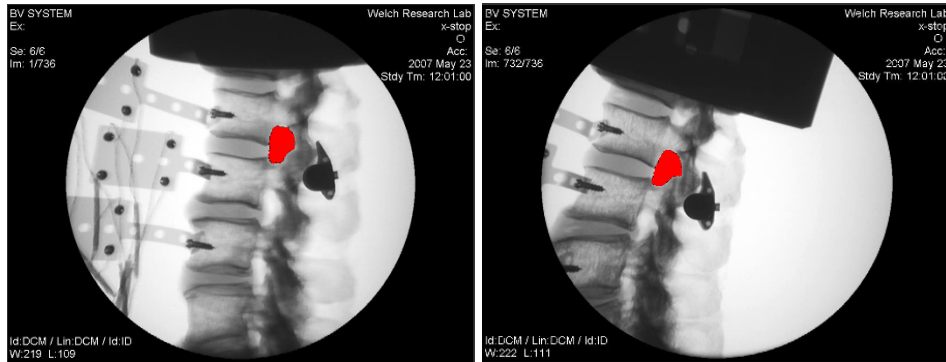

Figure 4: Segmented foramina cross sections (red regions) of the foramina cross sections before extension (left) and after extension (right).

Results and Discussion

Suppose the top left of the image is the origin of the coordinate system, and the spacing is 1×1. Table 1 shows the translation and the rotation angle for *L2* after applying flexion extension bending. Table 2 shows the translation of the instanta-

neous rotation center calculated from segmented *L*2 and *L*3, the area change of the foramina between *L*1 and *L*2. We observed that the flexion extension bending resulted in a reduced ROM corresponding to 10.4% of the ROM found in the control. However, the difference in foramina cross sectional area measured 5.6% between the first 5 flexion frames and the last 5 extension frames.

Table 1: Translation and rotation angle before/after extension of *L*2

	Centroid	$\cos^{-1}\left(\frac{\vec{n}_1 \bullet \vec{j}}{\|\vec{n}_1 \bullet \vec{j}\|}\right)$	Translation	Rotation Angle
before extension	(493.34, 377.73)	80.44°	(-215.72, 39.97)	-1.09°
after extension	(277.62, 417.69)	79.35°		

Table 2: Instantaneous rotation center (*L*2&*L*3) and foramina area change

	Instantaneous Rotation Center	Foramina Area (between *L*1, *L*2)	Translation	Area Change
before extension	(478.21, 440.20)	3425	(-242.16, 45.94)	5.6%
after extension	(236.05, 486.14)	3233		

ROM comparisons have been accurate in predicting the clinical efficacy of fixation hardware. However, the ability to maintain the foramina space under load has not currently been a priority to characterize. Interspinous process spacers, along with other motion preservation devices, require additional biomechanical parameters in order to characterize clinical behavior. The implanted level exhibited a major reduction in ROM but minor change in cross sectional foramina area between the two extremes. Effectiveness of such devices in extension bending is important from a translational medicine point of view and requires information beyond ROM measures alone.

References

1. Back.com, http://www.back.com/anatomy.html.

2. Malladi, R. and Sethian, J.A. (1998): "A real-time algorithm for medical shape recovery", *Int'l Conf. on Computer Vision*, pp. 304–310.

3. Sethian, J.A. (1999): *Level Set Methods and Fast Marching Methods (2nd edition)*, Cambridge University Press.

4. Yu, Z. and Bajaj, C.L. (2005): "Automatic Ultra-structure Segmentation of Reconstructed Cryo-EM Maps of Icosahedral Viruses", *IEEE Transactions on Image Processing*, Vol. 14, No. 9, pp. 1324-1337.